Simulation of a single-element rocket combustor using a non-adiabatic Flamelet model

Nikolaos Perakis [(1)], Christof Roth [(1)], Oskar J. Haidn [(1)]

[(1)]Chair of Turbomachinery and Flight Propulsion, Technische Universität München
Boltzmannstraße 15, 85748 Garching, Germany
nikolaos.perakis@ltf.mw.tum.de

KEYWORDS: CFD, Flamelet, methane, wall heat flux, non-adiabatic, equilibrium

ABSTRACT

In the present work a single-element rocket thrust chamber operated with gaseous methane (GCH_4) and gaseous oxygen (GOX) is investigated numerically by employing the tabulated chemistry models of chemical equilibrium and Flamelet. Due to the low chemical reaction rates present in hydrocarbon combustion, non-equilibrium effects are needed for the correct description of the flame. Since the Flamelet model includes non-equilibrium effects in form of scalar dissipation, it is considered to be superior to the equilibrium chemistry model (ECM) in case of CH_4/O_2 chemistry. For this reason a comparison of the two models was undertaken and their differences were identified. Apart from the standard “frozen” Flamelet model approach, which cannot predict recombination effects close to the wall, a non-adiabatic model developed by the authors was implemented for the simulation of the test case. Significant differences between the frozen and non-adiabatic methods are observed, especially in the vicinity of the cold chamber walls. Although physically more motivating, the non-adiabatic model appears to over-predict the heat released due to recombination reactions in the boundary layer, thereby leading to a high heat flux. Moreover, the effects of multi-pressure tabulation and of turbulence-chemistry interaction (TCI) are investigated. It is found that multi-pressure tabulation is not needed for low pressure operating points (20 bar), whereas the absence of TCI over-estimates the temperatures in the chamber and TCI should therefore be included.

NOMENCLATURE

h	: specific enthalpy [$\mathrm{J/kg}$]
p	: pressure [bar]
P	: Probability Density Function (PDF) [-]
$\dot{q}$	: heat flux [$\mathrm{W/m^2}$]
T	: temperature [K]
u	: velocity [$\mathrm{m/s}$]
x	: spatial coordinate [m]
Y	: species mass fraction [-]
Z	: mixture fraction [-]
Z''^2	: mixture fraction variance [-]
ζ	: normalized enthalpy [-]
ρ	: density [$\mathrm{kg/m^3}$]
χ	: scalar dissipation rate [$1/\mathrm{s}$]

Subscripts

ad	: adiabatic
min/max	: minimum/maximum
n	: normalized
ox/fu	: oxidizer/fuel
st	: stoichiometric

1. INTRODUCTION

Computational Fluid Dynamics (CFD) is a promising approach to improve the classic design and optimization processes of liquid rocket engine (LRE) thrust chambers. It can be used during the design phase to reduce the number of necessary tests and the redesign effort, thereby saving development time and lowering cost [1]. One area where CFD tools are typically employed is the layout of the heat management system. The tools used must be able to predict design parameters within a certain accuracy without being prohibitive to use due to computational cost. In order to achieve this, the relevant underlying physics must be modeled accurately. In addition, to increase the level of confidence in the numerical predictions, tools and models need to be validated with experimental data over the wide range of operating conditions that occur in rocket thrust chambers.
For this reason, in the framework of the research program SFB/TRR 40 "Fundamental Technologies for the Development of Future Space-Transport-System Components under High Thermal and Mechanical Loads", the Chair of Turbomachinery and Flight Propulsion (LTF) at the Technical University Munich conducted several hot firing tests of a lab-scale single-element rocket combustor using GCH_4/GOX as propellant combination. The test data has been made available for validating

numerical tools and models.
While there has been comprehensive research on hydrogen engines traditionally, worldwide activities have focused on methane as propellant recently. Since methane shows good performance and cooling properties, as well as low-toxicity and is space storable, it is an attractive option for future space transport systems [2]. Where an approach based on equilibrium chemistry has been successfully applied for the simulation of hydrogen fueled rocket combustors [2] [3], a model based on the Flamelet assumption is more suitable for methane engines, due to the comparatively larger chemical time scales, which result in a deviation from equilibrium. However most commonly used Flamelet models do not include the effect of heat-loss on the flame structure in terms of gas composition at low enthalpy levels. This is also the case for the 'native' model implemented in the commercial CFD Solver ANSYS Fluent [4], used for all CFD activities at the LTF. Therefore a model extension has been developed, allowing for the use of fully enthalpy depended Flamelet tables. The model used to generate the tables is presented by Perakis et al. [5]. In addition the effect of varying pressure on the flame structure is included and compared to a frozen approach that only includes pressure effects by density scaling.
The developed model enhancements are applied in the investigation of a single element lab-scale methane rocket combustor from the Technical University of Munich. The focus is the combustion, flow and heat transfer in the thrust chamber. Validation data is available in form of wall heat flux and axial pressure distribution.

2. TEST CASE

The investigated test case has been presented by the LTF as a part of a larger test campaign [7]. The combustion chamber is a modular heat sink hardware made of oxygen-free high conductivity copper. Due to the modular design the chamber length and configuration can be varied by inserting or removing different chamber segments. The configuration used for the presented results is depicted in Figure 1.
The total chamber length is 305 mm and the inner diameter is 12 mm. The nozzle has a conical shape with a throat diameter of 7.6 mm. Therefore the contraction ratio of the configuration is 2.5, which is close to actual flight hardware (Vulcain: 2.5, Aestus: 2.38) [6]. This ensures a similar Mach number in the combustor compared to that of the actual flight engines.
The hardware is equipped with several thermocouples along the chamber wall in axial direction. These are placed in short distance (1-3 mm) from the hot gas wall side and give an indication of the material heat up during the hot firing tests. The measurements are also used to reconstruct the experimental wall heat flux according to the inverse heat transfer method described in Celano et al. [7].
The wall pressure distribution is measured by nine pressure transducers mounted along the chamber wall. From their readings the axial evolution of the chamber pressure, which is related to the heat release, is obtained.
The injector used in the investigated configuration is a coaxial shear type injector. The oxidizer post tip is flush mounted with the faceplate, i.e. no recess is configured. The post tip is not tapered. The characteristic dimensions for the injector are given in Table 1. The element wall distance is equal to the outer radius of the hydrogen annulus, i.e. 3 mm.
The operating point examined in this work has a nominal chamber pressure of 20 bar and nominal oxidizer to fuel ratio of 2.2.

Table 1 Injector dimensions.

GOX diameter	d_i	=	4 mm
GFU outer diameter	d_o	=	6 mm
GOX post thickness	t	=	0.5 mm
Recess length	R	=	0 mm

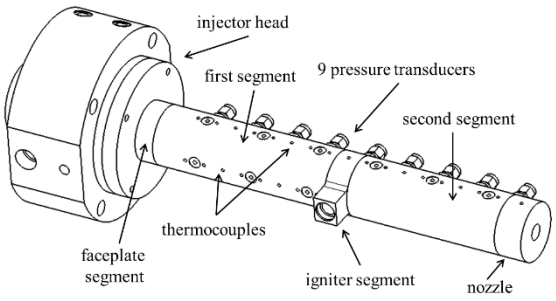

Figure 1: Sketch of the single element chamber assembly.

3. COMPUTATIONAL SETUP

For all simulations the Reynolds-averaged Navier-Stokes (RANS) equations are solved on a computational grid of approximately 92000 cells.

The domain contains the injector, chamber and nozzle and is treated as 2D-axisymmetric. At the inlet the mass flow rates from the experiments are given together with the injection temperatures. The outlet is set to a supersonic pressure outlet. At the combustor wall the temperatures from the thermocouple readings are set as boundary condition. This is a slight underestimation of the actual temperatures, but the effect on the simulation results is assumed to be negligible.

Turbulence is modeled using a two-layer k-ε model [4]. The wall is resolved to values of the dimensionless wall distance y+ of around one. In all calculations, the closure of the turbulence flux terms is done with a constant turbulent Prandtl and Schmidt number $Pr_t = 0.9$ and $Sc_t = 0.6$.

Turbulent combustion is modeled using tabulated chemistry based on either chemical equilibrium or a Flamelet assumption. The thermodynamic and transport properties are stored, in the most general case, in tables according to:

$$\tilde{\phi} = f(\tilde{Z}, \widetilde{Z''^2}, \tilde{\chi}_{st}, \tilde{p}, \tilde{h})$$

In case of the equilibrium model the scalar dissipation rate $\tilde{\chi}_{st}$ is taken to be zero and the effect of enthalpy on the gas composition is always included. For the Flamelet model heat-loss is accounted for in one of two ways. The frozen Flamelet takes the composition present at the adiabatic mixture enthalpy and generates additional levels by subtracting energy without influencing the mass fractions. All other tabulated quantities change in order to be thermodynamically consistent with the new enthalpy level. The non-adiabatic Flamelet approach takes into account the effect of heat-loss on the gas composition and therefore includes recombination effects occurring in the strongly cooled boundary layer near the combustor outer wall.

For the equilibrium as well as the Flamelet model the effect of pressure is either fully accounted for in the tabulation or included by pressure density scaling only. In the latter case the chemistry tables are generated at a reference pressure $\tilde{p}_{ref} = 20\ bar$. The gas density is then scaled during run time according to

$$\tilde{\rho} = \tilde{\rho}_{ref} \frac{\tilde{p}}{\tilde{p}_{ref}}$$

Hence in this case the effect of the pressure on the chemical composition of the hot gas is not included. Turbulence-chemistry interaction (TCI) is accounted for by use of the assumed beta PDF integration as presented by Kim et al. [8].

4. CHEMISTRY TABULATION

In the general case, the thermodynamic (temperature, specific heat capacity, density, species mass fractions, molecular weight) and transport (molecular viscosity, thermal conductivity) properties are saved in a multi-dimensional table during a pre-processing step. The independent variables of the table in the generalized case are, as mentioned in Section 3, the mixture fraction and its variance, the scalar dissipation, the pressure and the specific enthalpy.

For an efficient tabulation, and to ensure a linear lookup in all dimensions, the table is parametrized by modified variables.

In the case of mixture fraction, since it is defined between 0 and 1, no further modification has been carried out.

The mixture fraction variance $\widetilde{Z''^2}$ however is bound between 0 and $\tilde{Z}(1-\tilde{Z})$ and hence a function of the mixture fraction value for each table point. In the present work it is normalized according to

$$\widetilde{Z_n''^2} = \frac{\widetilde{Z''^2}}{\tilde{Z}(1-\tilde{Z})}$$

In the case of the scalar dissipation, it has been found that a logarithmic distribution is of benefit when dealing with the Flamelet model and for that reason the modified variable

$$\tilde{\chi} = \frac{\ln(\tilde{\chi}_{st}) - \ln(\tilde{\chi}_{st,min})}{\ln(\tilde{\chi}_{st,max}) - \ln(\tilde{\chi}_{st,min})}$$

has been utilized. In the case of chemical equilibrium, only the value for $\tilde{\chi}_{st} = 0$ is tabulated, whereas in the Flamelet model, $\tilde{\chi}_{st,min} = 10^{-4}\ 1/s$ and $\tilde{\chi}_{st,max} = 10^{4}\ 1/s$ were implemented to

ensure a sufficient coverage of the scalar dissipation in the chamber.
Similarly, a logarithmic distribution and normalization was chosen for the pressure as well:

$$\tilde{p}_n = \frac{\log \tilde{p} - \log \tilde{p}_{min}}{\log \tilde{p}_{max} - \log \tilde{p}_{min}}$$

Finally, the enthalpy levels in the table must ensure that all points of the CFD calculation are covered. For that reason, appropriate profiles for the minimal and maximal enthalpy profiles $h_{min}(\tilde{Z})$ and $h_{max}(\tilde{Z})$ have to be chosen. Typical profiles used in this work can be found in Perakis et al. [5] as well as in Figure 6. Since the enthalpy in each level is dependent on the value of the mixture fraction, a normalization is used and the normalized enthalpy levels ζ are given by

$$\zeta = \frac{h - h_{min}(\tilde{Z})}{h_{max}(\tilde{Z}) - h_{max}(\tilde{Z})}$$

It is important to understand the effect of each one of the lookup variables on the species concentration and temperature. A qualitative examination of these effects is undertaken in Figure 2. A generic table was created for CH_4/O_2 combustion with $T_{ox} = 275\ K$ and $T_{fu} = 270\ K$.

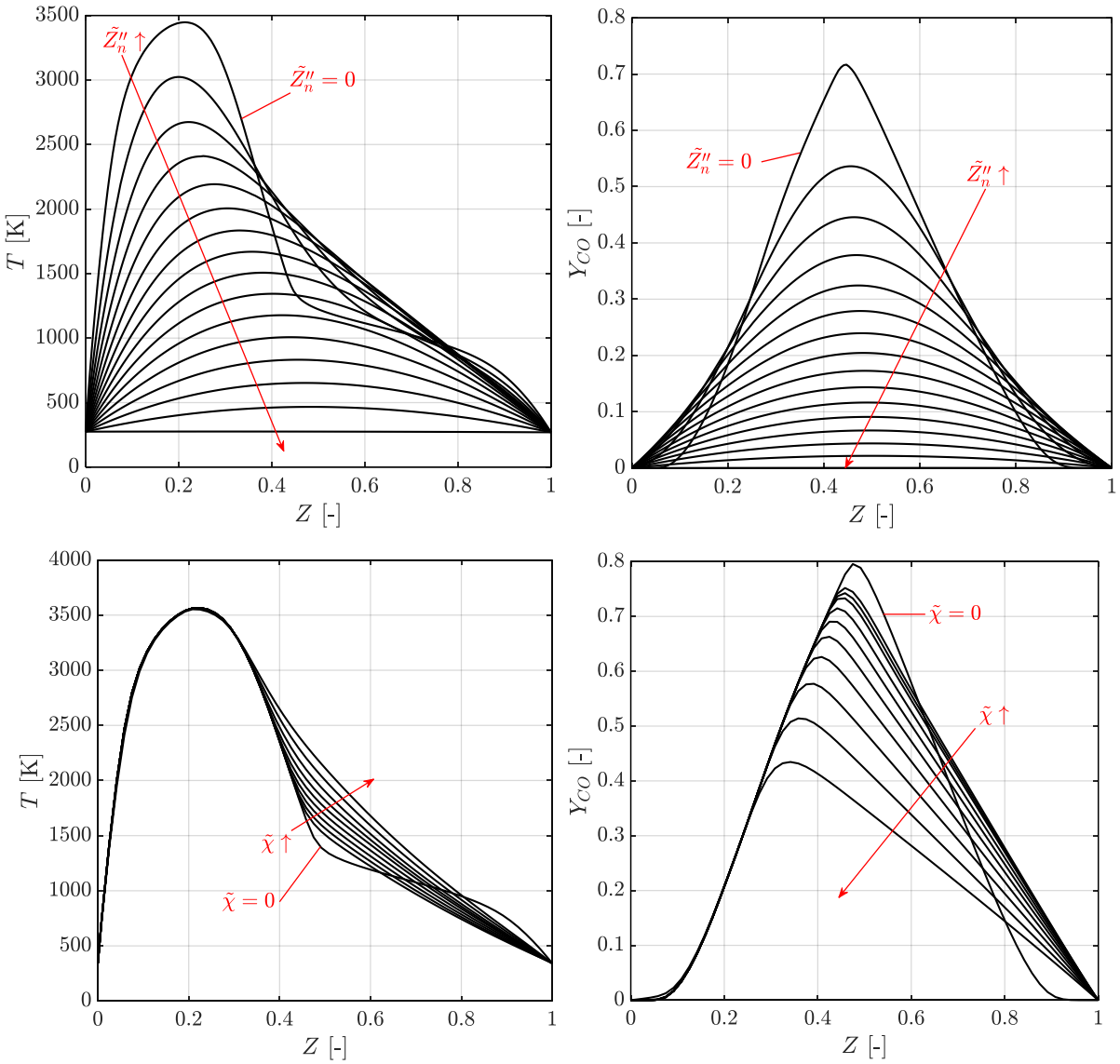

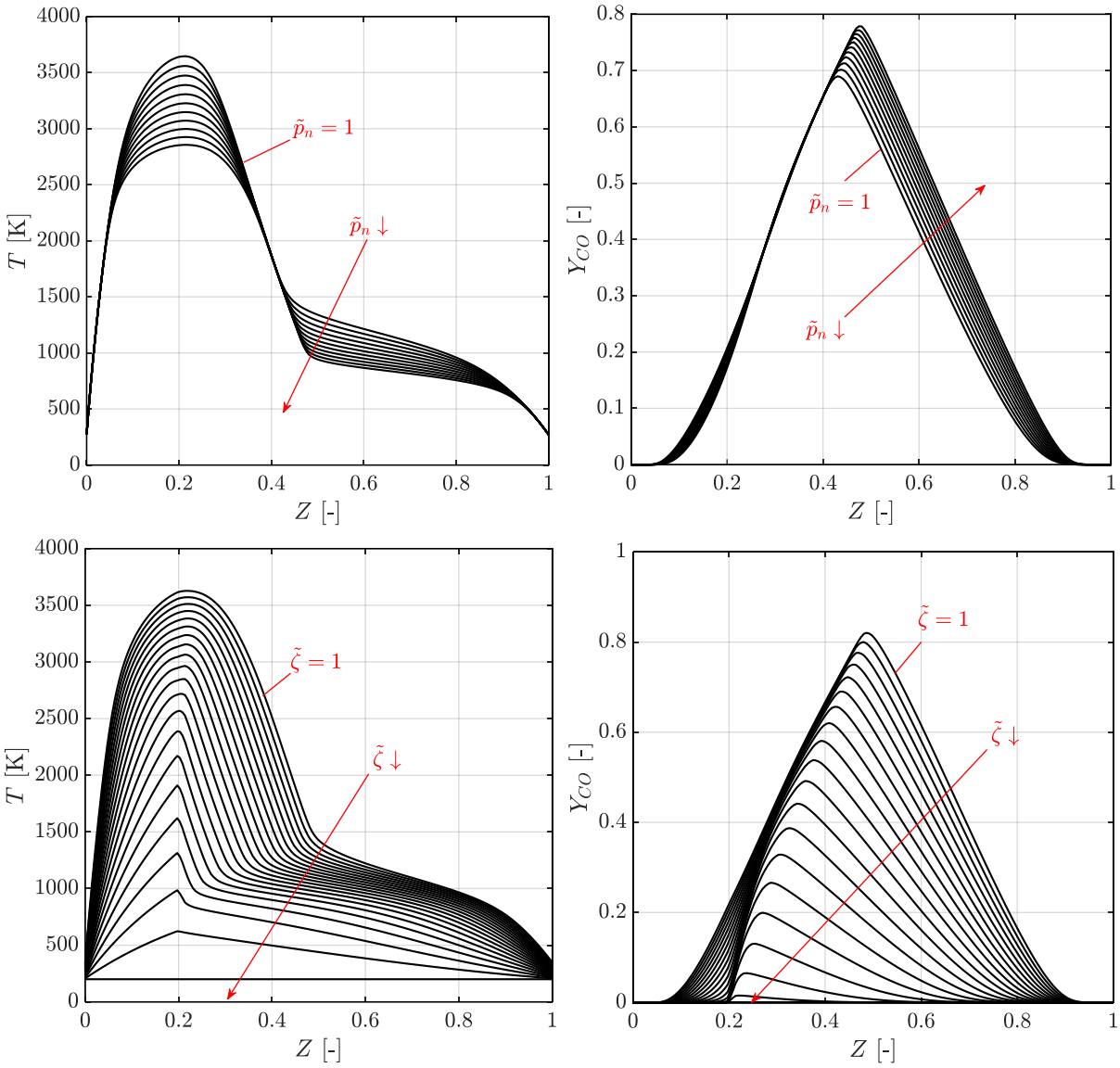

Figure 2: Effect of mixture fraction variance, scalar dissipation, pressure and enthalpy on temperature and CO mass fraction.

In the first row, the TCI influence on the tabulated values is illustrated. The results correspond to the adiabatic equilibrium solution at 20 bar and different levels of mixture fraction variance are plotted. In the case of maximal variance ($\widetilde{Z_n''^2} = 1$), the flame is completely extinct, and the profiles of temperature and species concentration correspond to an inert mixing

The effect of scalar dissipation in the second row also resembles a diffusion in the mixture fraction space. The laminar Flamelet is plotted here (zero mixture fraction variance), as in all subsequent figures. In the case of CH_4/O_2 combustion, the scalar dissipation mainly affects the fuel-rich region of the mixture. A significant difference between the equilibrium solution ($\tilde{\chi}_{st} = 0$) and the remaining eight levels (from $\tilde{\chi}_{st,min} = 10^{-4}\ 1/s$ to $\tilde{\chi}_{st,max} = 10^{4}\ 1/s$) is observed. Specifically the difference between the equilibrium level and the $\tilde{\chi}_{st,min} = 10^{-4}\ 1/s$ one appears to be quite abrupt. After further investigation, it was found that values down to $\tilde{\chi}_{st} \approx 10^{-9}\ 1/s$ would have to be tabulated to ensure a uniform change from the equilibrium level to the lowest Flamelet level. However in practice, no difference in the CFD solution was observed and hence $10^{-4}\ 1/s$ was chosen as the lowest value in order to reduce the computational time needed for

the table generation.
The effect of varying pressure was investigated in the range from 0.1 to 80 bar and is shown in the third row of Figure 2. As expected, a higher pressure leads to an increase of recombination reactions, which in turn produces a higher temperature. In the case of CH_4/O_2 the most important recombination is the one of CO and O to CO_2.
Finally, the effect of a reduced enthalpy environment compared to the adiabatic conditions is illustrated in the fourth row of Figure 2. Specifically, a lower enthalpy leads to a decrease in temperature but also to a decrease in CO concentration. The lower enthalpy (which is expected close to the boundary walls) leads to a recombination of radicals, which can be captured by the equilibrium and the non-adiabatic Flamelet models.

5. RESULTS

5.1 Multi-pressure tabulation and TCI

The effects of a multi-pressure tabulation and the inclusion of TCI in the form of a mixture fraction variance were investigated using the ECM. Specifically, four cases were identified resulting from the combination of single- and multi-pressure tables with and without TCI. In the case of single-pressure tables, the tabulated values correspond to 20 bar (the nominal pressure of the examined operating point), whereas for the no-TCI case, the variance was set to 0 in the whole domain.
In order to quantify the differences between the different models, the pressure and heat flux profiles in the combustion chamber and nozzle are illustrated in Figure 3, where they are compared to the experimental values. All four models appear to produce vary similar pressure profiles, and underestimate the static pressure in the combustion chamber by approximately 1 bar compared to measured values. In the nozzle no significant differences are visible but the absence of pressure transducers does not allow a comparison with the experiment. When it comes to the heat-flux profiles an interesting observation can be made. The heat flux level appears to be much higher than the experimental one, and this can be identified as the reason for the lower pressure. Due to the high heat loss through the wall, the energy in the hot gas is reduced, leading to a lower temperature and hence lower pressure level. The number of tabulated pressure levels appears to be irrelevant for the heat flux level in the chamber. This is expected, since the pressure does not vary significantly during combustion and hence multi-pressure effects are negligible. In the nozzle however, a measureable difference in the heat flux can be observed. Since the pressure drops from 19 bar down to almost 1 bar, the varying pressure affects the recombinations in the nozzle and the heat release. Hence, it can be seen that in simulations where the expansion in the nozzle is investigated, a multi-pressure table should be used.
Including TCI on the other hand has a significant effect on the heat flux level in the chamber. Specifically, it appears that the heat flux maximum is shifted further downstream when TCI is modeled and the heat flux level is also reduced. The lower heat flux is expected since the temperature values in the case of no TCI are higher as shown in Figure 2. This can also be confirmed when examining the contour plots in Figure 4. A significantly higher temperature and thinner flame is found in the no-TCI case which explains the higher heat flux. The heat flux maximum usually indicates the point where the heat release ends and hence a shift upstream in the no-TCI case suggests a better mixing and therefore an earlier end of combustion. A validation of this assumption can be seen in Figure 4, since the flame front (represented by the white line corresponding to the stoichiometric mixture fraction) is shorter in the case of no-TCI, hinting to a better mixing. Despite the big influence in the combustion chamber, the TCI does not seem to affect the flow in the nozzle. This is due to the fact that the gas is almost completely mixed when entering the nozzle and therefore the mixture fraction variance is close to zero.
After having established the impact of multi-pressure tabulation and TCI on the hot gas flow, a conclusion was drawn that for the specific test case, a multi-pressure tabulation is unnecessary and hence only one pressure level is included in all following calculations. TCI on the other hand appears to be non-negligible and for that reason it was decided to include it

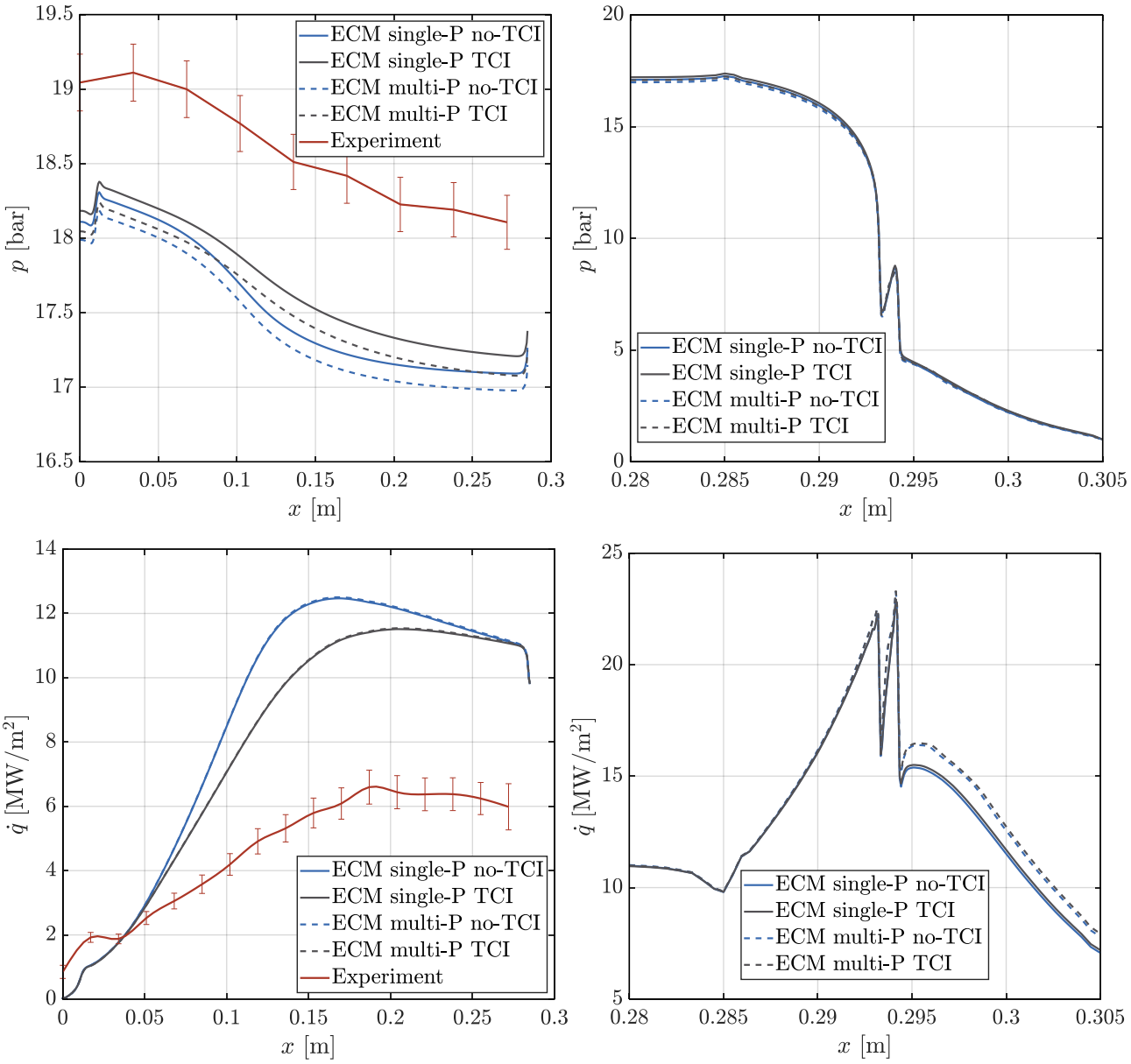

Figure 3: Pressure (up) and heat flux (down) profiles in the combustion chamber (left) and nozzle (right) for the ECM model.

5.2 Frozen vs non-adiabatic Flamelet

The effect of non-adiabatic Flamelet tabulation has been shown in theory by Perakis et al. [5] but it is important to see how the two models differ when applied to the simulation of a CH_4/O_2 rocket thrust chamber. The classic frozen model Flamelet has been used in several cases with success leading to heat flux levels matching the experimental ones with good agreement, is however physically not so motivating due to the absence of recombination reactions in the vicinity of cooled walls. This is also the main motivation behind the development of the non-adiabatic Flamelet model. For the present comparison, a single pressure level is used in the tabulation and TCI is included. The ECM results are also shown in Figure 5 for reference.

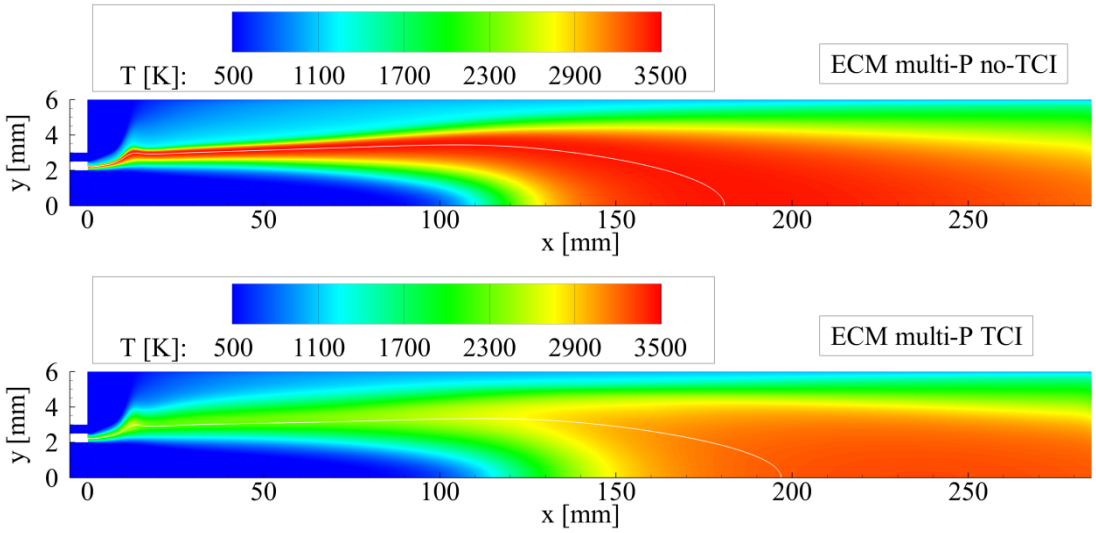

Figure 4: Temperature contour in the combustion chamber for the ECM multi-P case without (up) and with (down) TCI.

The pressure and heat flux profiles produced by the frozen Flamelet seem to match the experimental values with good accuracy. In the case of the non-adiabatic Flamelet however, a lower pressure and much higher heat flux compared to the experiment is predicted. In fact, the heat flux profile is closer to the ECM one than to the frozen Flamelet one. This is expected, since the ECM also includes non-adiabatic effects and is simply one "slice" of the non-adiabatic Flamelet table (the one corresponding to $\tilde{\chi}_{st} = 0$). Although the heat flux level is higher than the experimental values, the profile form is quite similar. Specifically, both the experimental and the non-adiabatic profile increase up until 0.2 m downstream of the faceplate and then appear to drop, indicating the end of combustion and the increase of the thermal boundary layer. The frozen Flamelet on the other hand appears to fail in predicting the correct mixing in the chamber, leading to a heat flux profile that keeps increasing until the beginning of the nozzle.

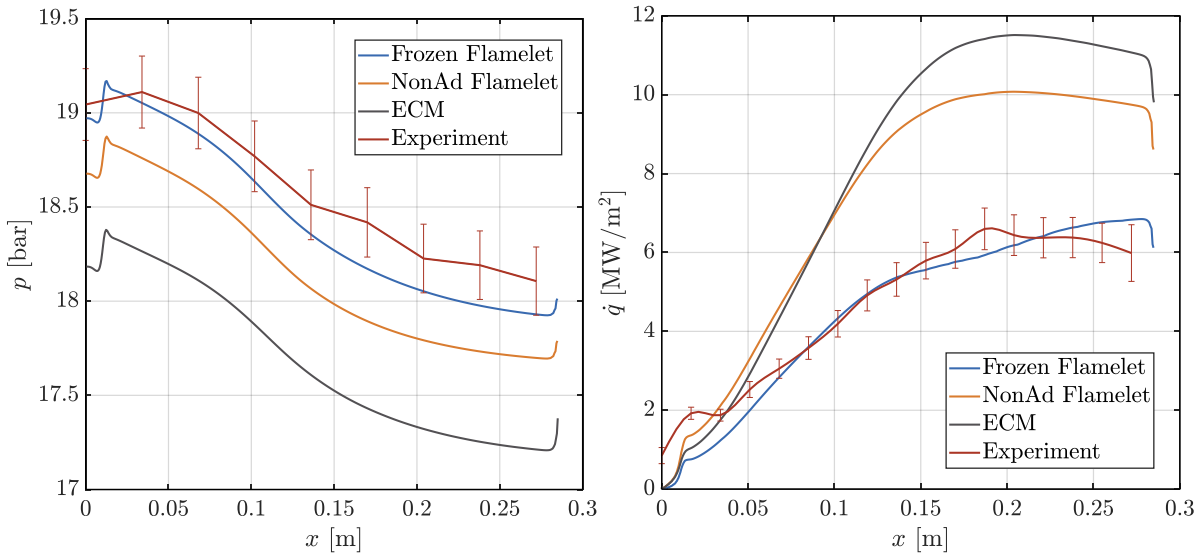

Figure 5: Pressure (left) and heat flux (right) profiles for the frozen Flamelet, non-adiabatic Flamelet and ECM at the combustion chamber wall.

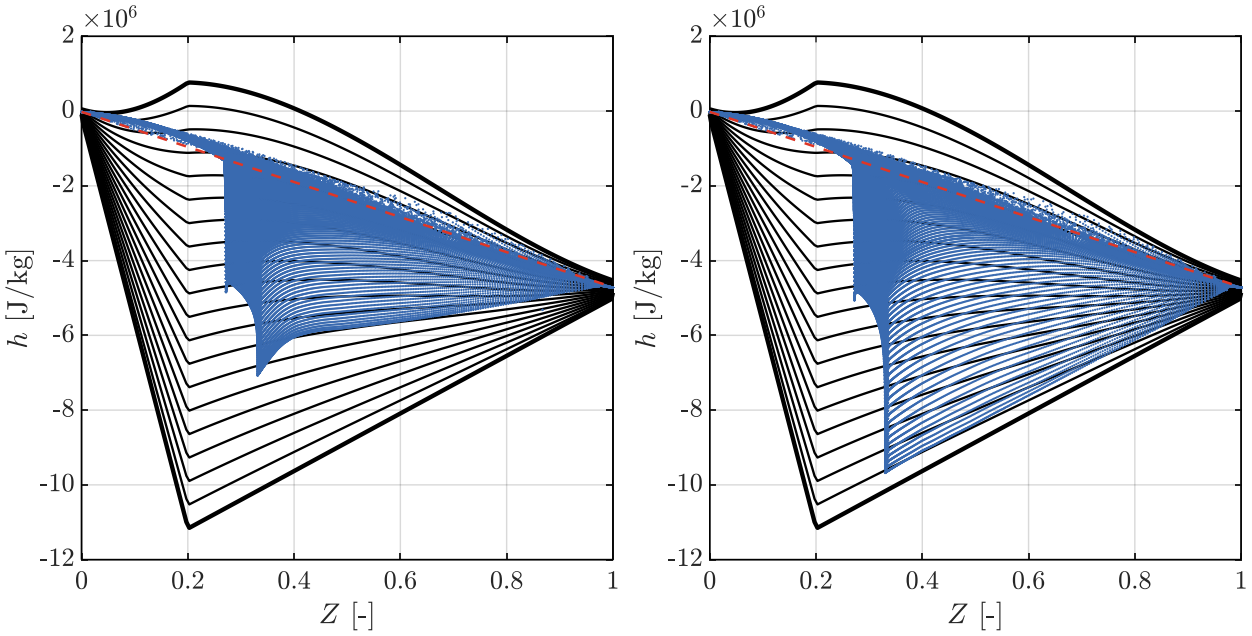

Figure 6: Enthalpy scatter plots for the frozen (left) and non-adiabatic Flamelet models.

The higher heat flux predicted by the non-adiabatic model also influences the thermodynamic points that are required to be stored in the lookup table. Figure 6 illustrates a scatter plot of the enthalpy in all of the computational cells in the mixture fraction space. Apart from these points, the enthalpy levels used for the tabulation are also included with the thicker lines representing the h_{min} and h_{max} profiles. The dashed line represents the adiabatic profile. In the oxygen-rich region ($Z < 0.2$), most of the points are clustered in the vicinity of the adiabatic profile, since they are located away from the wall. Since the outer annulus of the injector is where methane is injected from, the gas concentration close to the wall is fuel-rich. This explains why many points with enthalpy values below the adiabatic one are found in the $Z > 0.31$ region. ($Z = 0.31$ corresponds to the global O/F of 2.2 for this test case). Although the chosen minimum enthalpy profile seems to cover the frozen Flamelet points with sufficient buffer, it marginally captures the non-adiabatic points. This is due to the higher heat flux predicted at the wall which further reduces the boundary cells enthalpy compared to the frozen case.

The temperature fields for the two models are depicted in Figure 7. In the core flow, no significant differences can be identified. The flame temperature in the frozen case appears to be minimally higher but in general, no indicator for the massive difference in heat flux can be given by simply looking at the contour plot. In order to understand the origin of the high heat flux in detail, the temperature profile along a line normal to the chamber wall is shown in Figure 8. The location of the line is at 250mm from the faceplate, which is close to the end of the chamber. In the left subfigure, the temperature profile over the entire radius of the chamber is plotted, whereas the right subfigure focuses on the boundary layer. It is evident, that the frozen and the non-adiabatic models have very similar profiles over almost the entire radius, whereas the ECM shows a measurable difference. The deviation from the ECM lies on the non-equilibrium effects induced by the scalar dissipation, whereas the similarity between the two Flamelet models is due to the almost adiabatic conditions far away from the wall. Zooming into the wall however (right subfigure), it appears that the discrepancies between the frozen and non-adiabatic Flamelet models increase, and that the non-adiabatic solution approaches the ECM one. Close to the wall, the lower enthalpy is responsible for the initiation of recombination reactions which are not captured by the frozen model leading to a larger descripancy in the temperature and its gradient. Moreover, the magnitude of the scalar dissipation decreases closer to the wall and for that reason the ECM and the non-adiabatic Flamelet tend to converge to a single line

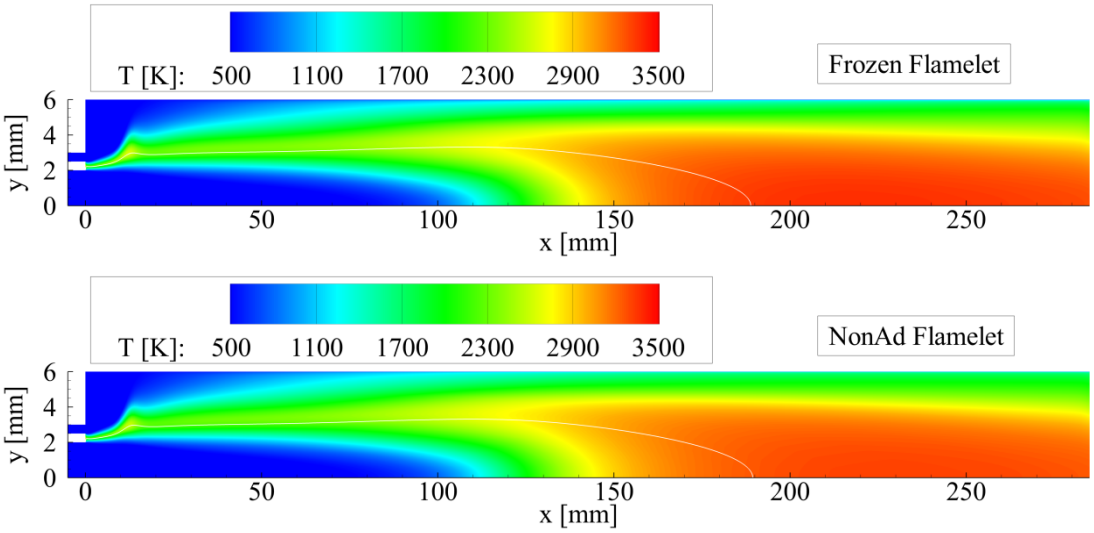

Figure 7: Temperature contour plots for the frozen (up) and non-adiabatic (down) Flamelet models.

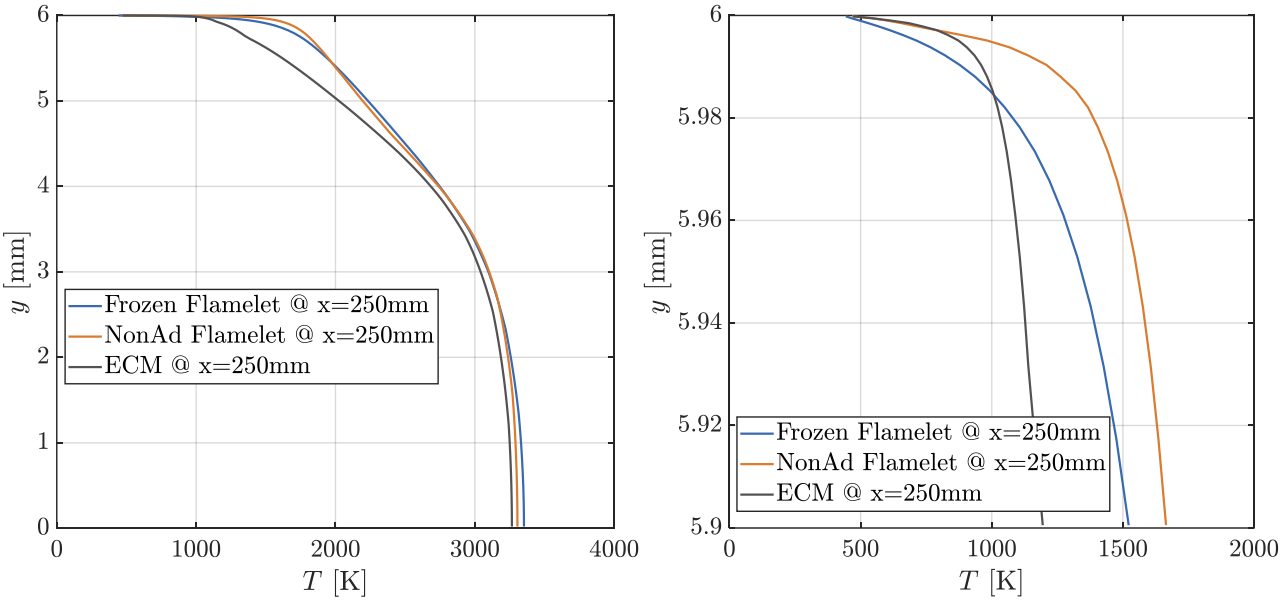

Figure 8: Temperature profile normal to the chamber wall at x=250 mm.

The origin of the different temperature gradients is the disparity in tabulated species concentration for the two models. This is confirmed when examining the species profiles as done in Figure 9 and Figure 10. It is evident that the recombination of CO to CO_2 and the recombination of OH to H_2O are greatly amplified in the case of the non-adiabatic Flamelet. Close to the wall, the concentration of CO significantly drops compared to the frozen case, whereas CO_2 and H_2O rise. In fact the profiles of the non-adiabatic Flamelet seem to resemble the ECM ones.

Although the presence of recombination reactions close to cooled walls appears physically motivating, it seems that the non-adiabatic Flamelet model over-predicts their reaction rate. Close to the wall, the Flamelet model tends to be almost identical to the ECM, since the scalar dissipation goes to zero and hence near-equilibrium concentrations are predicted, leading to a very high heat flux. Possibly the extension of the Flamelet table by an additional variable to include further non-equilibrium effects also in the vicinity of the wall could improve the Flamelet model.

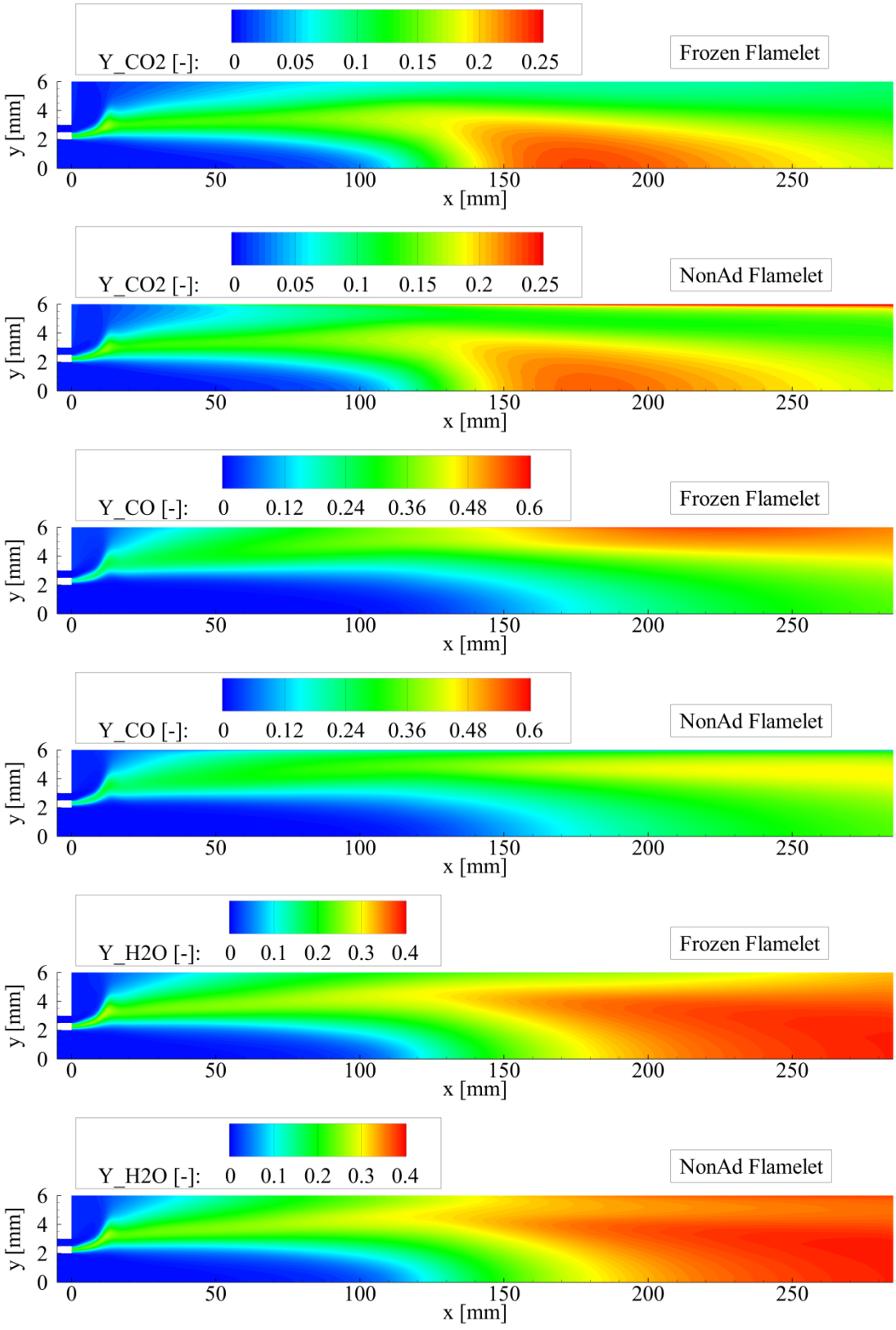

Figure 9: Species contour plots for the frozen and non-adiabatic Flamelet models: CO_2 (up), CO (middle) and H_2O (down).

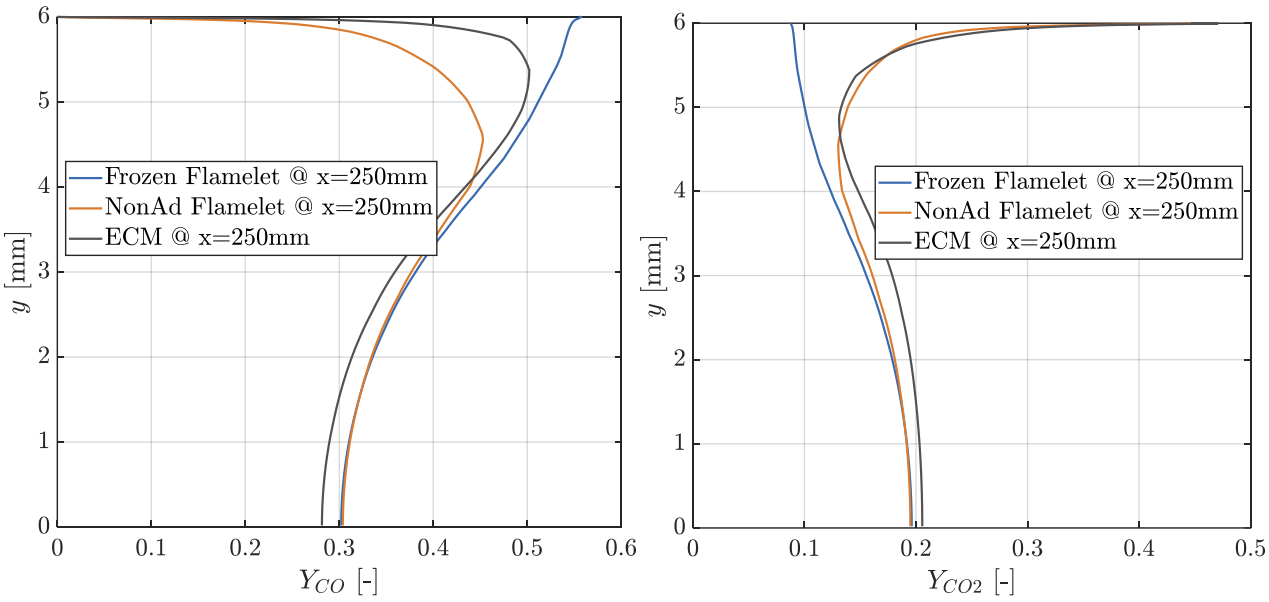

Figure 10: Species profiles normal to the wall at x=250 mm (CO left and CO_2 right).

6. CONCLUSION AND OUTLOOK

The Flamelet model is a very promising method for the simulation of turbulent combustion in applications where non-equilibrium effects become significant. Its application in CFD simulations of rocket combustion engines with hydrocarbons as propellants reduces the computational time compared to more thorough approaches such as finite rate chemistry. The idea that an extension of the Flamelet model to include non-adiabatic effects is needed to accurately predict the wall heat loads is common in the CFD community and the present work attempted to investigate this assumption.

First, investigations on an equilibrium model were carried out to see the effect of multi-pressure tabulation and turbulence-chemistry interaction on the flame structure. It was found that the multi-pressure tabulation does not affect the heat flux profiles in the combustion chamber, but does have an effect in the nozzle portion of the engine, where the expansion takes place. The TCI on the other hand was found to be important in the chamber, since its absence leads to an overprediction of the temperature and the heat flux. In general the heat flux stemming from the ECM was found to be much higher than the experimental one, which is expected, since CH_4/O_2 chemistry is too slow to be sufficiently described by an equilibrium model.

Using a single-pressure tabulation and TCI in the form of a beta-PDF, the frozen and non-adiabatic Flamelet model were directly compared to each other. It was found that the heat flux profile in the non-adiabatic Flamelet solution is much higher than the experimental one, whereas the frozen Flamelet captures the heat flux level with good accuracy. The pressure in the non-adiabatic case is also lower than the experimental one, which is caused by the large amount of wall heat loss due to the overestimated wall heat flux.

The main difference between the two models appears to be in the boundary layer, whereas the core flow is quite similar. In fact close to the wall, the low enthalpy leads to excessive recombination reactions in the non-adiabatic model. The low magnitude of the scalar dissipation in the boundary layer makes the non-adiabatic Flamelet model behave like the ECM. This is the reason for the high heat flux values experienced.

Although the non-adiabatic Flamelet is theoretically more physically motivating, since it can capture recombination effects close to cooled walls, it definitely exaggerates the production of CO_2 and H_2O and leads to non-physical wall loads. Further investigations have to be carried out in order to evaluate whether the model can be improved by choosing another method of tabulating the non-equilibrium effects, i.e. by substituting or modifying the scalar dissipation rate.

ACKNOWLEDGEMENTS

Financial support has been provided by the German Research Foundation (Deutsche Forschungsgemeinschaft – DFG) in the framework of the Sonderforschungsbereich Transregio 40.

REFERENCES

[1] J. Lin, J. S. West, R. W. Williams, K. P. Tucker and J. D. Chenoweth, "CFD Code Validation of Wall Heat Fluxes for a GO2/GH2 Single Element Combustor," in *Joint Propulsion Conference*, Tucson, 2005.

[2] H. Burkhardt, M. Sippel, A. Herbertz and J. Klevanski, "Kerosene vs Methane: A Propellant Tradeoff for Reusable Liquid Booster Stages," *Journal of Spacecraft and Rockets,* vol. 41, no. 5, pp. 762-769, 2004.

[3] B. Ivancic, H. Riedmann and M. Frey, "Validation of Turbulent Combustion Models for the 3D-Simulations of Liquid H2/O2 Rocket Combustors," in *Space Propulsion Conference*, Bordeaux, 2012.

[4] H. Riedmann, B. Kniesner, M. Frey and C. D. Munz, "Modeling of combustion and flow in a single element GH2/GO2 combustor," *CEAS Space Journal,* vol. 6, no. 1, pp. 47-59, 2014.

[5] Fluent ANSYS, "Ansys Fluent theory guide," ANSYS Inc. USA, 2011.

[6] N. Perakis, C. Roth and O. J. Haidn, "Development of a non-adiabatic Flamelet model for reacting flows with heat loss," in *Space Propulsion*, Sevilla, Spain, 2018.

[7] S. Silvestri, M. P. Celano, G. Schlieben, O. Knab and H. O. J, "Experimental Investigation on Recess Variation of a Shear Coax Injector," in *Space Propulsion*, Rome, Italy, 2016.

[8] G. Schmidt, Technik der Flüssigkeits-Raketentriebwerke, Munich: DaimlerChrysler Aerospace, 1999.

[9] P. M. Celano, S. Silvestri, J. Pauw, N. Perakis, F. Schily, D. Suslov and O. Haidn, "Heat flux evaluation methods for a single element heat-sink chamber," in *EUCASS*, Krakov, 2015.

[10] S. K. Kim, M. Joh, H. S. Choi and T. S. Park, "Multidisciplinary simulation of a regeneratively cooled thrust chamber of liquid rocket engine: Turbulent combustion and nozzle flow.," *International Journal of Heat and Mass Transfer,* vol. 70, pp. 1066-1077, 2014.